frontiers | Frontiers in Earth Science

TYPE Original Research
PUBLISHED 15 June 2023
DOI 10.3389/feart.2023.1191049

OPEN ACCESS

EDITED BY
Zhibo Zhang,
University of Science and Technology Beijing, China

REVIEWED BY
Yang Xiao,
Xi'an University of Science and Technology, China
Bo Tan,
China University of Mining and Technology, China
Chunliu Liu,
Anhui University of Technology, China
Ge Huang,
Liaoning Technical University, China

*CORRESPONDENCE
Jiafeng Fan,
symkyfjf@163.com

RECEIVED 21 March 2023
ACCEPTED 31 May 2023
PUBLISHED 15 June 2023

CITATION
Fan J (2023), Effects of CO_2 injection factors on preventing spontaneous coal combustion in coal mine gobs: a simulation approach.
Front. Earth Sci. 11:1191049.
doi: 10.3389/feart.2023.1191049

Effects of CO_2 injection factors on preventing spontaneous coal combustion in coal mine gobs: a simulation approach

Jiafeng Fan*

State Key Laboratory of Coal Mine Safety Technology, China Coal Technology and Engineering Group Shenyang Research Institute, Shenfu Demonstration Zone, Fushun, China

The spontaneous combustion of residual coal in the gob seriously threatens the safety of coal mining. Injecting CO_2 into the gob not only prevents the residual coal from spontaneous combustion but also realizes CO_2 storage in the mined areas. Injection flux and burial depth of the port are crucial for CO_2-preventing fire in coal mine gobs. In this study, the distribution of the oxidation zone in the Tanyaoping coal mine was field-measured, and the coal oxidation kinetic model was built by the adiabatic test. Then, a 3-D mathematical model was constructed based on the conditions of the 5011 working face by COMSOL Multiphysics. Furthermore, the coupled effects of the two factors on the distribution of the oxidation zone were investigated. Increases in both injection flux and burial depth result in a decrease in the oxidation zone volume. The reasonable ranges of the injection flux and burial depth are 540–720 $m^3 h^{-1}$ and 30–40 m, respectively. These results provide some guidelines on how to prevent the spontaneous combustion of residual coal in mine gobs.

KEYWORDS

coal, spontaneous combustion, CO_2 injection, oxidation zone, oxidation kinetic model

1 Introduction

China is the largest producer of coal in the world. Coal mining normally faces several types of accidents that can cause environmental disruption, fatalities, and equipment loss (Zhang et al., 2021; Li et al., 2022). The reaction between coal and O_2 at low temperatures usually results in spontaneous combustion and uncontrolled coal fires (Zhang et al., 2023). During underground coal mining, spontaneous combustion of residual coal in the mine gob often leads to a wide range of secondary disasters, such as methane explosions, carbon monoxide generation, and ventilation disorders. The oxidation process of residual coal in the gob is extremely complex. High-mechanized technology, especially coal caving mining, results in considerable coal resources left in the gob. However, it is necessary to keep enough fresh air through the airways and working face for human survival and methane dilution. Therefore, the residual coal in the gob is exposed to continuous O_2 and has the possibility of spontaneous combustion. The hazardous areas of self-ignition in the gob depend on many factors, such as air leakage, thickness of residual coal, and the advanced rate of the working face (Zhu and Wen, 2023). Normally, the "three zones" (the cooling zone, oxidation zone, and suffocation zone) in the gob are determined based on the distribution of O_2 concentration in the gob area (Ma et al., 2020).

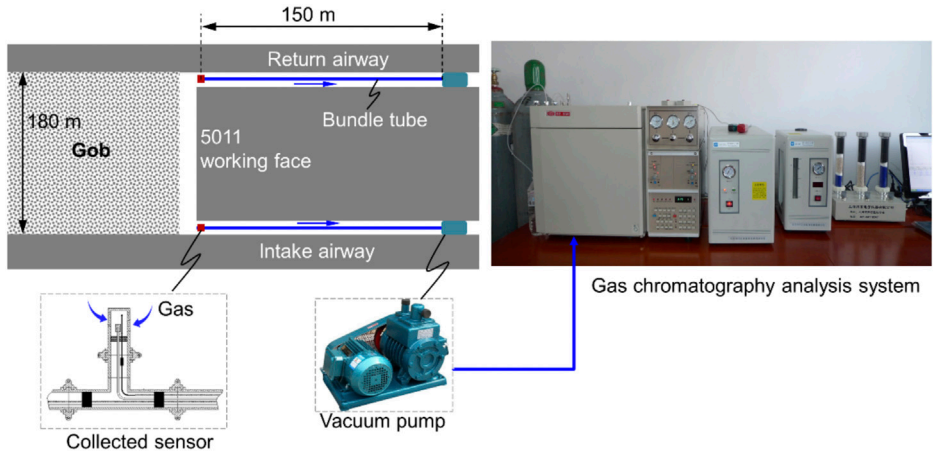

FIGURE 1
Measurement of O_2 concentration in the gob.

Spontaneous combustion of coal is influenced by coal oxidation reactions, heat accumulation, and the characteristics of porous media (Si et al., 2021). Therefore, many technical solutions were presented to prevent coal from spontaneous combustion and inhibit coal fire, which normally focus on two aspects: isolating coal active sites from O_2 and cooling the temperature (Dou et al., 2022). The present strategies can be broadly classified as uniform pressure ventilation (Lu et al., 2017), grouting (Zhang et al., 2018), spray inhibitors (Lu et al., 2020; Sun et al., 2022), pumping inert gas (Zhu and Wen, 2023), and injecting gel foam or gel (Lu et al., 2018; Lu et al., 2021; Han et al., 2022; Huang et al., 2022). CO_2 is an inert gas and can dilute the O_2 concentration and protect the coal from heat release. Furthermore, broken coal can absorb CO_2 and thus saved from oxidation (Guan et al., 2018). With the advancement of the working face, the volume of the mine gob increases. The resistance of internal airflow is small, and the porosity is large. Thus, the coal mine gob is an ideal location for storing CO_2. Injecting CO_2 into the gob can achieve the dual benefits of fire prevention and CO_2 storage.

This study is based on the actual conditions of the 5011 working face of the Tanyaoping coal mine. To achieve the fire prevention of residual coal in the gob by injecting CO_2, the oxidation zone was calculated by mathematical simulation using COMSOL Multiphysics. This simulated result without CO_2 injection was verified to be reasonable by comparing it with the field measurement. By studying the effect of the injection flux and burial depth of the injection port on the oxidation zone, the superior injection parameters were determined.

2 Overview of the 5011 working face

The Tanyaoping coal mine is located in Lvliang city, China. The recoverable coal seams consist of 5# and 10# coal seams. The 5011 working face is in coal seam 5# and adopts the "U" ventilation method. Coal seam 5# is the main production seam

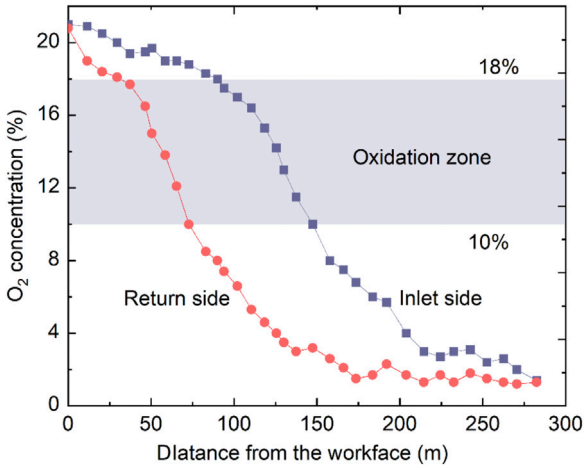

FIGURE 2
O_2 concentration of measured points in the intake and return airways.

and is around 4.4 m thick. The width and design length are 180 and 2,000 m, respectively. The width and height of the intake and return airways are 5 and 4.5 m, respectively. The thickness of the residual coal that remains in the mined area, that is, the gob, is about 0.4 m. The mined coal has a spontaneous combustion tendency.

As shown in Figure 1, two sensors were fixed in the intake and return airways to collect the gas. The monitoring system was based on the measurement of bundle tubes. With the advancement of the working face, O_2 concentrations at different buried depths were drawn out through the bundle tubes using a vacuum pump. A gas chromatography analysis system was used to analyze the O_2 concentrations of the collected bags. Figure 2 shows the measured O_2 concentration values in the intake and return airways. The O_2 concentrations at the observation points decrease with increasing buried depth. According to the actual

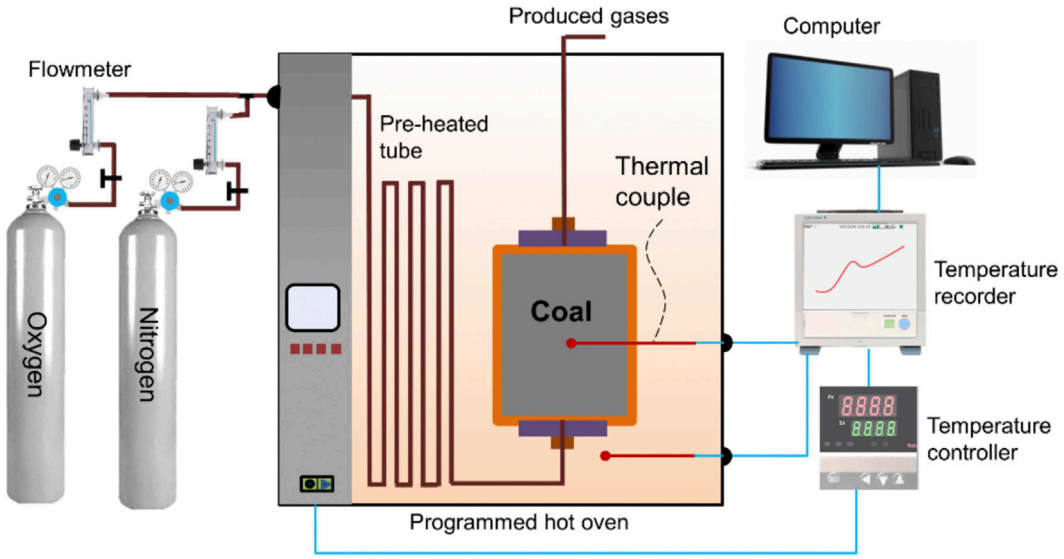

FIGURE 3
Schematic representation of the adiabatic oxidation test.

condition and other studies, the "three zones" were divided by using an O_2 concentration of 10%–18% (Ma et al., 2020). The O_2 concentration at the point in the intake airway decreased to 18% and 10% at 90 and 147 m, respectively. For the measured point in the return airway, the buried depths of O_2 concentrations of 18% and 10% are 30 and 73 m, respectively. Normally, there are three parameters to determine the "three zones" in the gob: the air leakage velocity, O_2 concentration, and heating rate (Deng et al., 2018). However, the O_2 concentration is the most accessible and was, therefore, applied in this study to judge the oxidation zone.

3 Coal oxidation kinetic model

Coal exothermic processes under low temperatures include three forms: physical adsorption, chemical adsorption, and chemical reactions (Liang et al., 2021). Chemical adsorption and chemical reactions are recognized as the main reasons for promoting the self-heating of coal under low temperatures (Zhang et al., 2019; Qu et al., 2023). Although partially active functional groups are self-reacting, a significant amount of heat will be released from the coal–O_2 reaction. Therefore, a linear relationship between the O_2 consumption rate and heat generation rate is generally considered to exist, expressed as follows:

$$q = r\Delta H, \tag{1}$$

where q is the heat generation rate of the coal reaction ($W{\cdot}m^{-3}$); ΔH is the coal oxidation heat ($J{\cdot}mol^{-1}$); and r is the O_2 consumption rate ($mol{\cdot}m^{-3}{\cdot}s^{-1}$).

Based on the coal oxidation dynamics theory, another major influence on coal oxidation is temperature, which increases, causing the activation of functional groups, i.e., the exothermic intensity increases with increasing temperature. Most of the models on O_2 consumption in the previous studies were based on the Arrhenius equation, expressed as follows:

$$r = Ac_o \exp\left(-E/RT\right), \tag{2}$$

where A is the pre-exponential factor (s^{-}); E is the activation energy ($J{\cdot}mol^{-1}$); R is the gas constant ($8.314\ J\ mol^{-1}{\cdot}K^{-1}$); c_o is the O_2 concentration (%); and T is the temperature (K). The kinetic parameters in Equation 2 are normally obtained from the adiabatic oxidation test.

As shown in Figure 3, the coal sample was mined from the 5011 working face of the Tanyaoping coal mine. Moisture, ash, volatile matter, and fixed carbon of coal are 7.64, 2.21, 26.24, and

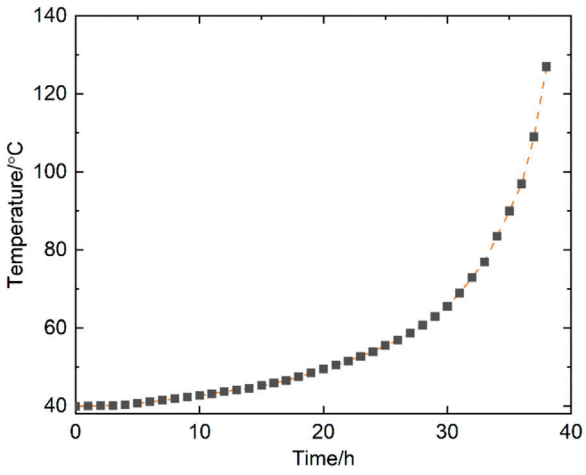

FIGURE 4
Temperature profile versus time under adiabatic conditions.

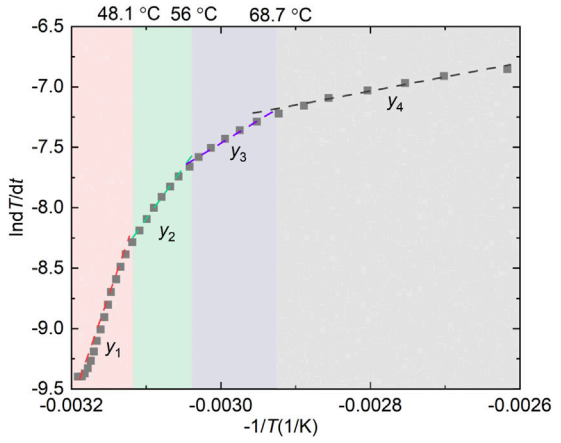

FIGURE 5
Fitting of lndT/dt versus $-1/T$.

63.19, respectively. Elements of C, H, O, and N of coal are 63.61, 4.86, 0.81, and 30.69, respectively. Approximately 220 g of coal particles (0.2–0.45 mm) were prepared and naturally filled into the reaction vessel. The sample was dried in N_2 at 105°C for 5 h and then cooled to 40°C under a N_2 atmosphere (Wang et al., 2010). Once the temperature was stable, the mixed gases with 21% O_2 were injected into the reaction vessel at 10 mL min^{-1}. It should be ensured that the oven temperature is synchronized with the coal temperature using the temperature controller. The change in coal temperature over time was recorded using the recorder for later analysis. Figure 4 shows the temperature profile versus time of the adiabatic oxidation test.

Under the adiabatic conditions, the coal sample was subjected to accelerated self-oxidation so that the heat released in the last step was completely converted to internal energy, which can be described by Equation 3 as follows:

$$q = \rho_c C_{pc} \frac{dT}{dt} = r\Delta H = \Delta H A c_o \exp(-E/RT), \tag{3}$$

where ρ_c is the density of coal (kg·m^{-3}) and C_{pc} is the specific heat capacity of coal (J·kg^{-1}·K^{-1}). Equation 4 can be rearranged by taking the natural logarithm, which is expressed as follows:

$$\ln \frac{dT}{dt} = \ln \frac{\Delta H A c_o}{\rho_c C_{pc}} - \frac{E}{R} \cdot \frac{1}{T}, \tag{4}$$

$$y = \begin{cases} y_1 = -17230x + 45.476 \quad R^2 = 0.9796 \quad (x < 48.1), \\ y_2 = -6910.4x + 13.353 \quad R^2 = 0.9933 \quad (48.1 < x < 56), \\ y_3 = -3955.9x + 4.3786 \quad R^2 = 0.9937 \quad (56 < x < 68.7), \\ y_4 = -2343.1x - 0.3393 \quad R^2 = 0.9974 \quad (x > 68.7). \end{cases} \tag{5}$$

The relationship between lndT/dt and $-1/T$ shown in Figure 5 is a nonlinear positive correlation, which does not follow the standard Arrhenius equation, and this phenomenon also appears in other studies (Zhang et al., 2020; Yoruk and Arisoy, 2022). It is difficult to fit the curve with one or two straight lines. The curve was divided into four stages with three break points of 48.1, 56, and 68.7°C. In each stage, lndT/dt and $-1/T$ exhibit good linearity, as shown in Equation 1. The slope of the fitting line in each stage presents the value of $-E/R$, and the intercept is the value of $\ln \Delta H A c_0/\rho_c C_{pc}$. The apparent activation energies of the four stages are 143.25, 57.45, 32.89, and 19.48 kJ mol^{-1}, respectively. Accordingly, the pre-exponential factors of the coal sample are 2.53×10^{20}, 2.83×10^{6}, 358.31, and 3.2 s^{-1}, respectively. In the numerical calculation, different E and A are invoked based on the coal temperature for the heat generation model.

4 Numerical simulation

The process of spontaneous combustion of residual coal in the gob area will involve heat transport and generation, O_2 consumption and transport, CO_2 emission and migration, and gas airflow. As shown in Figure 6, all the involved equations are interrelated based on the fluid-solid-thermal coupling (Xia et al., 2016; Zhang et al., 2019; Qi et al., 2021). The continuity equation and the momentum conservation equation are as follows:

$$\frac{\partial(\varepsilon \rho_g)}{\partial t} + \nabla(\rho_g \mathbf{U}) = 0, \tag{6}$$

$$\frac{\partial(\varepsilon \rho_g \mathbf{U})}{\partial t} + \nabla \cdot (\varepsilon \rho_g \mathbf{U}\mathbf{U}) = -\varepsilon \nabla p + \nabla \cdot (\varepsilon \boldsymbol{\tau}) + \varepsilon \mathbf{F} - \frac{\varepsilon^2 \mu}{K} \mathbf{U}, \tag{7}$$

where ρ_g is the density of air (kg·m^{-3}); ε is the porosity of gob; t is the time (s); $\mathbf{U}$ is the seepage air velocity vector (m·s^{1}); p is the static pressure (Pa); $\boldsymbol{\tau}$ is the stress tensor (Pa); μ is the air viscosity (Pa s); K is the permeability (m^2); and $\mathbf{F}$ is the gravitational body force (N·m^{-3}).

The relationship between porosity and permeability is expressed as

$$K = \frac{d\varepsilon^3}{150(1-\varepsilon)^2}, \tag{8}$$

where d is the particle size (mm). With the working face advanced, the stress status of overlying strata is damaged, and the roof-bed formation collapses. The overlying strata are vertically divided into a caving zone, fissure zone, and bent deformation zone based on the differences in the balance status and re-compaction degree of the damaged strata (Qin et al., 2016). Therefore, it is a significant challenge to build mathematical models with reasonable permeability and porosity in the gob area. According to the observation of the mine pressure, the compaction bulking factor, k, of the gob follows the law (Xia et al., 2015):

$$\varepsilon = 1 - \frac{1}{k}, \tag{9}$$

$$k = k_{p,\min} + (k_{p,\max} - k_{p,\min}) \cdot \exp\{-a_1 d_1 \cdot [1 - \exp(\xi_1 \cdot a_0 d_0)], \tag{10}$$

where $k_{p,\min}$ and $k_{p,\max}$ are the initial bulking factors before and after compacting in the gob area, respectively, (1.15 and 1.5). a_0 and a_1 are the decay ratios of the bulking factor in the dip and strike directions of the working face, respectively, (0.268 and 0.0368 m^{-1}). d_0 and d_1 are the distances between the point (x,y) in the gob and the working face and coal pillar, respectively. ξ_1 is the adjustment factor controlling the distribution pattern of the model, 0.233.

The local thermal non-equilibrium is considered in the energy equation of conservation, which is given by

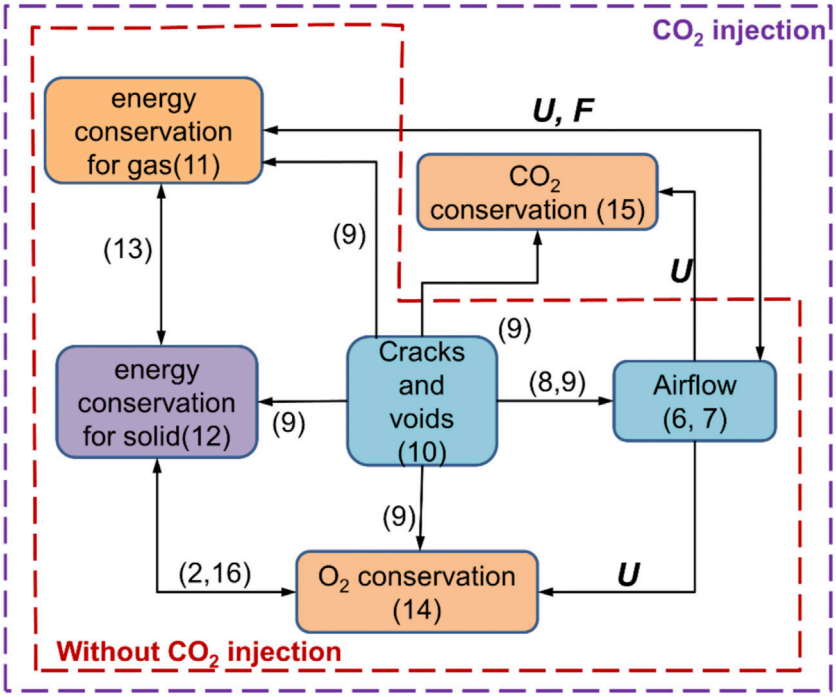

FIGURE 6
Main conservation equations of modeling.

$$\text{For gas, } \varepsilon\rho_g C_{pg}\frac{\partial T_g}{\partial t} + \rho_g C_{pg}\mathbf{U}\nabla T_g = \varepsilon\nabla\left(\lambda_g \nabla T_g\right) + q_{gc}, \tag{11}$$

$$\text{For solid, } (1-\varepsilon)\rho_c C_{pc}\frac{\partial T_c}{\partial t} = (1-\varepsilon)\nabla(\lambda_c \nabla T_c) - q_{gc} + (1-\varepsilon)q_o, \tag{12}$$

where C_{pg} is the specific heat capacity of air (J·kg^{-1}·K^{-1}); λ_g and λ_c are the thermal conductivities of air and coal, respectively (W·m^{-1}·K^{-1}); T_g and T_c are the temperatures of air and coal, respectively (K); q_o is the heat generation rate of coal (W·m^{-3}) obtained using Equation 3; q_{gc} is the solid–gas heat exchange around coal particles (W·m^{-3}), which has

$$q_{gc} = h_{gc}a\left(T_c - T_g\right), \tag{13}$$

where h_{gc} is the convective heat transfer coefficient (W·m^{-2}·K^{-1}), indicating the heat exchange between coal and pore air; a is the specific surface area, that is, the exposed area of coal particles per unit volume (m^{-1}).

O_2 conservation is a unique consideration without CO_2 injection. However, we must consider the conservation of O_2 and CO_2 for fire prevention by injecting CO_2 into the gob, which is expressed as follows:

$$\varepsilon\frac{\partial c_o}{\partial t} + \nabla(\mathbf{U}c_o) = \nabla(\varepsilon D\nabla c_o) + r_o, \tag{14}$$

$$\boldsymbol{\varepsilon}\frac{\partial c_m}{\partial t} + \nabla(\mathbf{U}c_m) = \nabla(\varepsilon D\nabla c_m) + r_m, \tag{15}$$

where c_m is the concentration of CO_2 (mol·m^{-3}); D_o and D_m are the effective diffusivities of O_2 and CO_2, respectively (m^2·s^{-1}); and r_o is the O_2 consumption rate (mol·m^{-3}·s^{-1}). r_m is the CO_2 generation rate (mol·m^{-3}·s^{-1}) of coal oxidation, whose ratio to r_o is 0.1 (Taraba et al., 2014). The oxidation reaction of residual coal in the gob is affected by working face advance. Based on Equation 2, r_o can be expressed as

$$r_o = wr, \tag{16}$$

where w is the influence coefficient of working face advance.

In addition, to ensure the normal operation of modeling, the following main assumptions are supplemented (Ma et al., 2020; Zhang et al., 2022):

(i) The effects of moisture transport and evaporation are not considered.
(ii) Thermal conductivity and heat capacity of coal and gas are independent of other parameters.
(iii) The transfer of heat in the gob merely involves convection and conduction, and the radiative transfer is not taken into account.
(iv) The gas in the gob is incompressible.

According to the actual conditions of the 5011 working face, the corresponding geometric model has been established. COMSOL Multiphysics software was applied to simulate the oxidation process of residual coal in the mine gob. The whole model consists of four parts: the mining area, the inlet airway, the return airway, and the working face. The cross-sectional area of both the inlet and return airways is 22.5 m^2, and the cross-sectional area of the working face is 25 m^2. The length of the inlet and return airways is 5 m. The length of the working face is set as 220 m, and

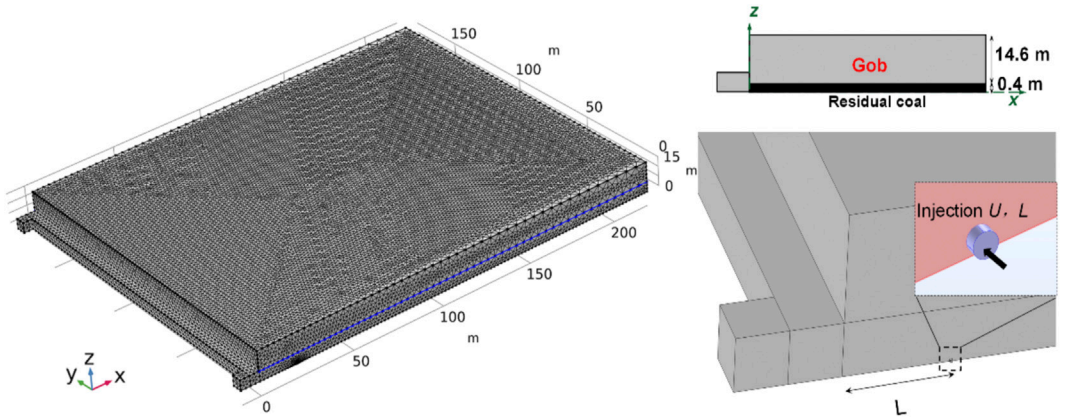

FIGURE 7
Geometric model and meshing.

TABLE 1 Main parameters applied in the numerical simulation.

Parameter	Item	Value	Unit
A_0	Pre-exponential factor	40	kJ·mol^{-1}
E	Apparent active energy	320	s^{-1}
ρ_a	Density of air	1.225	kg·m^{-3}
ρ_c	Density of coal	1300	kg·m^{-3}
c_a	Specific heat capacity of air	1007	J·kg^{-1}·K^{-1}
c_c	Specific heat capacity of coal	1210	J·kg^{-1}·K^{-1}
λ_a	Thermal conductivity of air	0.02	W·m^{-1}·K^{-1}
λ_c	Thermal conductivity of coal	0.21	W·m^{-1}·K^{-1}
μ	Viscosity	1.87×10^{-5}	Pa·s
D_o	O_2 diffusion coefficient	1.76×10^{-5}	m^2·s^{-1}
D_m	CO_2 diffusion coefficient	1.6×10^{-5}	m^2·s^{-1}
h_{gc}	Convective heat transfer coefficient	11	W·m^{-2}·K^{-1}
ΔH	Coal oxidation heat	380,000	J·mol^{-1}
w	Influence coefficient of working face advance	0.9	-

the length and height of the gob area are 180 and 15 m, respectively. For the condition without CO_2 injection, grid independence was checked by carrying out three sets of grids. Eventually, after considering the CPU time and the sensitive parameter, 34,954 mesh blocks are divided among this model, including 32,389 mesh blocks in the gob area. The mesh blocks of the models for CO_2 injection were slightly larger than those without CO_2 injection. The time step was set as 1 h. As shown in Figure 7, the CO_2 injection port was a round tube with a radius of 0.2 m and a length of 0.2 m. Two parameters, injection flux (U, m^{3}h^{-1}) and injection port burial depth (L, m), were considered to investigate the performance of CO_2 injection in preventing residual coal fires. The parameters used in the simulations are listed in Table 1. The boundary and initial conditions used in the mathematical model are illustrated in Table 2.

5 Results and discussion

5.1 Analysis of the oxidation zone without CO_2 injection

As shown in Figures 8A, B, the porosities and permeabilities of the gob near the working face and pillars are larger than those of the

TABLE 2 Boundary and initial conditions of the mathematical model.

	Types	Positions	Values
Boundary conditions	Inlet	x = −5 m	Velocity: 0.7 m s^{-1} (1050 m^3 min^{-1})
		y = 0–5 m	Temperature: 20°C
		z = 0–5 m	O_2 concentration: 9.7 mol m^{-3}
		x = L	Velocity: U
		y = −0.2 m	Temperature: 20°C
		z = 0.1 m (circle)	CO_2 concentration: 44.6 mol m^{-3}
	Outlet	x = −5 m	Free outflow
		y = 115 m–120 m	
		z = 0–5 m	
	Wall	Other surfaces	Temperature: 20°C
Initial conditions	Temperature	Entire domain	20°C
	(Seepage) velocity		0
	CO_2 concentration		0
	O_2 concentration		9.7 mol m^{-3}

inner zone due to the mining process. Fresh air enters the working face from the inlet airway with a velocity of 0.7 m s^{-1}, and more than 90% of the ventilation flux passes through the working face and then flows into the return airway. The airflow streamlines in the gob area, normally from the windward zone near the inlet airway to the zone near the return airway. The airflow velocity near the working face is larger than that in the inner zone due to the smaller forced-convection resistance.

With the deepening of the gob, the O_2 concentration gradually decreases. As shown in F8(e), on the side of the inlet airway, the fresh air from the intake airway enters the gob and flows toward the deep. However, gases with low O_2 concentrations flow from the deep to the return airway. Therefore, the O_2 concentration near the side of the return airway shows a more rapid decline than that of the intake airway.

This distribution of the oxidation zone has been observed in many other field measurements and simulations (Xia et al., 2015; Chu et al., 2019; Xu et al., 2020). Coal near the working face undergoes a strong oxidation reaction because of the abundant O_2, accompanied by the release of heat. We can find that the high-temperature zone is located on the windward side of the oxidation zone, as shown in Figure 8C. It is due to the fact that O_2 was consumed in the high-temperature zone, causing fewer O_2 molecules to enter the interior of the gob. Therefore, it is difficult to transport enough O_2 to the inner zone, resulting in a low concentration of O_2 within the area. The distribution of CO_2 in the gob is the opposite of the distribution of O_2 because most of the CO_2 in the gob is derived from low-temperature oxidation of residual coal, as shown in Figure 8D. The overall CO_2 values are much lower than those of O_2. The CO_2 concentration near the working face is lower than that in the inner zone due to the dilution of airflow seepage.

Figure 8E is a three-dimensional distribution of O_2 concentration in the gob area. The O_2 concentration in the upper area in the same vertical direction is slightly higher than that in the lower area. The volume of the oxidation zone without CO_2 injection is calculated to be 121,000 m^3. The average width of the oxidation band is 45 m. Figure 8F shows the range comparison of the oxidation zones (z=0.2 m) between the field measurement and simulation. The two results show good alignment. It indicates that the numerical simulation can reflect the performance of the self-ignition of the residual coal in the gob.

5.2 Analysis of the base case with CO_2 injection

The base case of U = 540 m^3 h^{-1} and L = 20 m was calculated, and the distributions of O_2, CO_2, and temperature in the gob area are shown in Figure 9. CO_2 injection has the properties of a displacement effect on the air leakage, a dilution effect on the O_2 distribution, and a cooling effect on the high-temperature zone. Therefore, the spontaneous combustion of residual coal is delayed or prevented. CO_2 injection can dilute the O_2 concentration. CO_2 concentration is much higher than O_2 concentration downstream of the injection port. The oxidation zone on the inlet airway side moved significantly toward the injection port, and the width of the oxidation zone decreased significantly. CO_2 was continually mixed with leaked O_2, and the dilution effect on the O_2 distribution was gradually attenuated. The high-temperature zone under CO_2 injection was a smaller area than that without CO_2 injection. CO_2 also suppresses the maximum temperature in the gob. It indicates that CO_2 can restrict the self-ignition of coal. In addition, the area of the oxidation zone for CO_2 injection on the surface z = 0.2 m is 1300 m^2, much smaller than that without CO_2

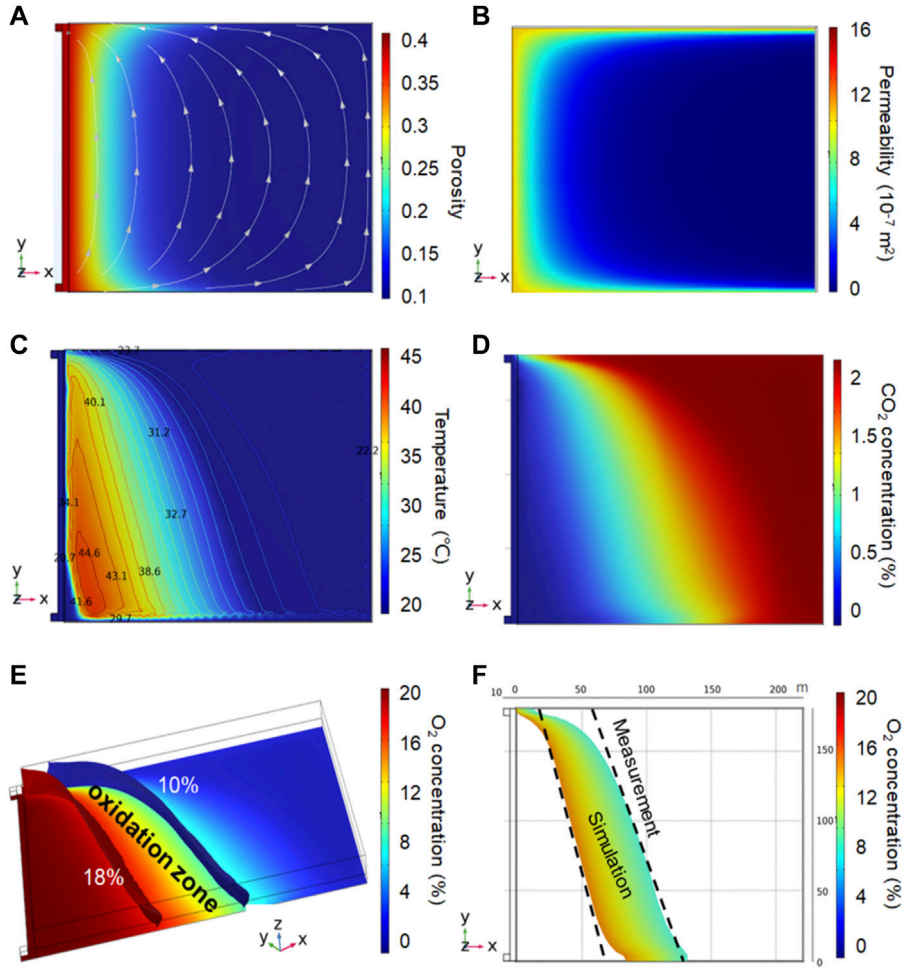

FIGURE 8
Numerical simulation without CO_2 injection: **(A)** porosity and airflow seepage at z=0.2 m, **(B)** permeability distribution at z=0.2 m, **(C)** temperature distribution at z=0.2 m, **(D)** CO_2 distribution at z=0.2 m, **(E)** 3-D oxidation zone, and **(F)** oxidation zone at z = 0.2 m.

injection, which is 7400 m^2. However, the volumes of the oxidation zone with and without CO_2 injection are 63,000 m^3 and 121,000 m^3, respectively. The injection port is located near the bottom, causing a large amount of CO_2 cluster in the lower area and, therefore, not easily diluting O_2 in the upper area. As a result, the width of the oxidation zone in the upper area is much greater than that of the lower area.

5.3 Effect of the CO_2 injection flux

Based on the base case and the corresponding simulation without CO_2 injection, the effects of the CO_2 injection flux on the prevention of residual coal fires were analyzed. The assumed CO_2 injection fluxes are 180, 360, 540, 720, 900, and 1080 m^3 h^{-1}, respectively. Figure 10 shows the oxidation zone in the gob for different CO_2 injection fluxes at L=20 m. An increase in the injection flux weakens the O_2 concentration in the gob and increases the displacement effect. When $U \geq 180$ m^3 h^{-1}, the higher pressure of the intake airway and gravity suppress the injected CO_2, which flows along the lower side of the gob in the direction of airflow seepage, as shown in Figure 11. At U= 180 and 540 m^3 h^{-1}, CO_2 concentrations in the upper zone of the gob are much lower than those in the bottom zone. Because the CO_2 injection fluxes (≤1080 m^3 h^{-1}) are smaller than the air flux from the intake airway (1050 m^3 min^{-1}). CO_2 injection hardly affects the air leakage streamlines, and thus, the high CO_2 areas at different U values are extremely similar. With the increase in CO_2 injection flux, the overall distribution of the oxidation zone moves toward the working face. The oxidation zone in the lower gob area moves toward the upwind side of the injection port when $U \geq 0$. As wind speeds increase, the distance between the iso-surfaces increases by 10% to 18%, reducing the volume of the oxidation zone. The volumes of the oxidation zone at U = 180, 360, 540, 720, 900, and 1080 m^3 h^{-1} are 89,000, 62,500, 43,000, 2,950, 24,000, and 23,000 m^3 at L=20 m, respectively. Therefore, when $U <$ 900 m^3 h^{-1}, the volume of the oxidation zone decreases with the injection flux, and when $U >$ 900 m^3 h^{-1}, the volume changes little as flux increases. This phenomenon also appears in other cases with different L values.

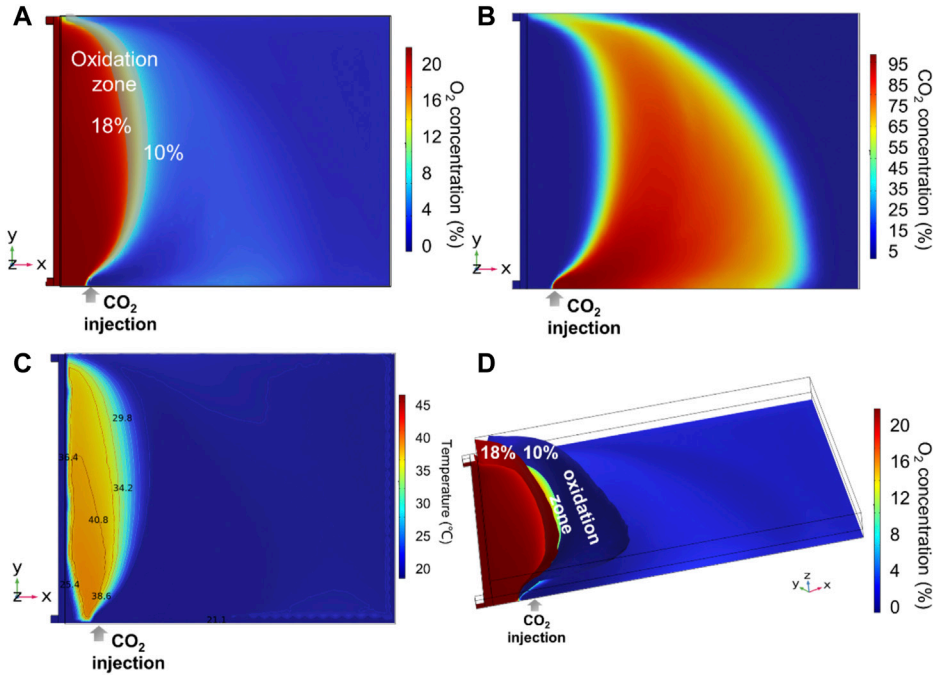

FIGURE 9
Numerical simulation with CO_2 injection (L = 20 m and U = 540 $m^3\ h^{-1}$): **(A)** oxidation zone at z = 0.2 m, **(B)** CO_2 distribution at z = 0.2 m, **(C)** temperature distribution at z = 0.2 m, and **(D)** 3-D oxidation zone.

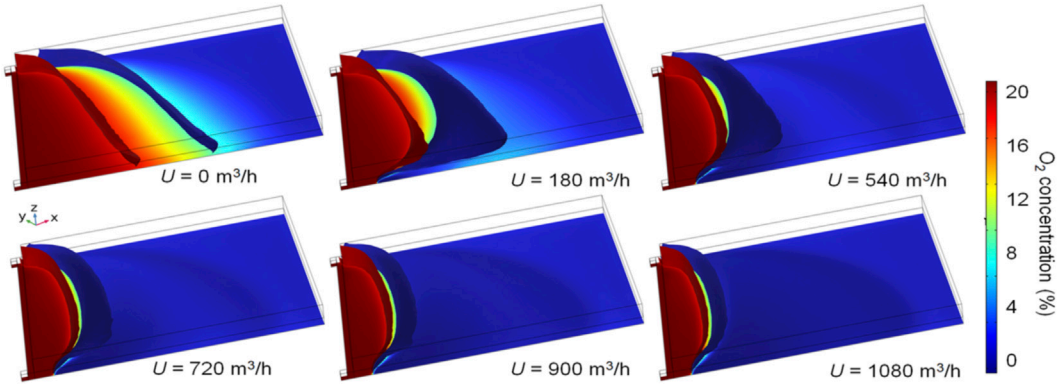

FIGURE 10
Simulated oxidation zone with different injection fluxes at L = 20 m.

5.4 Effect of the CO_2 injection location

Figures 12, 13 show O_2 and CO_2 distributions in the gob with different burial depths at U = 540 $m^3\ h^{-1}$. Once CO_2 is injected, the oxidation zone on the inlet side is significantly reduced. This is because the high CO_2 concentration near the injection port effectively dilutes O_2. The closer the inlet port is to the working face, the closer the oxidation zone on the inlet side is to the working face, and the weaker the effect of the O_2 concentration in the upper area of the inlet side being displaced by CO_2. It is due to the high leakage strength near the working face and a large amount of fresh air that suppresses CO_2 diffusion by the dilution effect. Therefore, as shown in Figure 13, the smaller L is, the lower the CO_2 concentration within the gob. At L = 10, 20, and 30m, the CO_2 concentration in the upper area of the gob is low. Moreover, as the burial depth of the injection port increases, the airflow leakage from the working face is small, and CO_2 can migrate to the upper area without high resistance. The volumes of the oxidation zone at L= 10, 20, 30, 40, 50, and 60 are 65,000, 43,000, 27,000, 23,000, 19,200, and

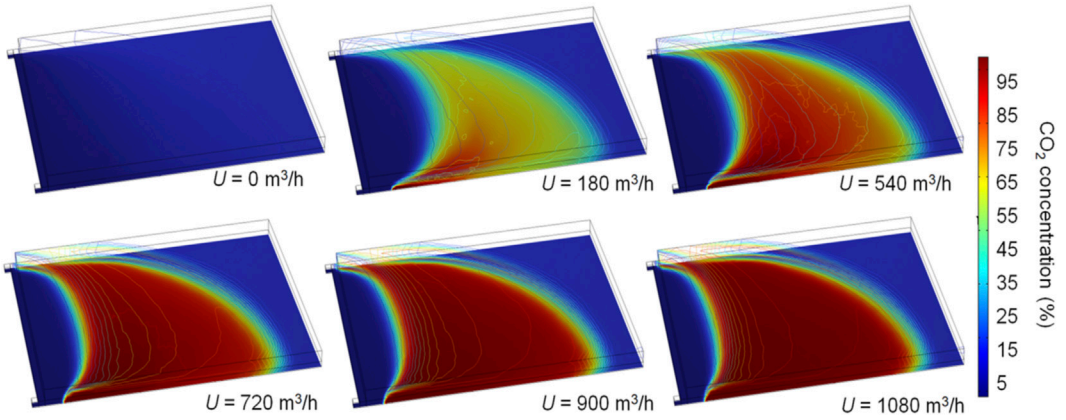

FIGURE 11
Simulated CO_2 distribution with different injection fluxes at L = 20 m.

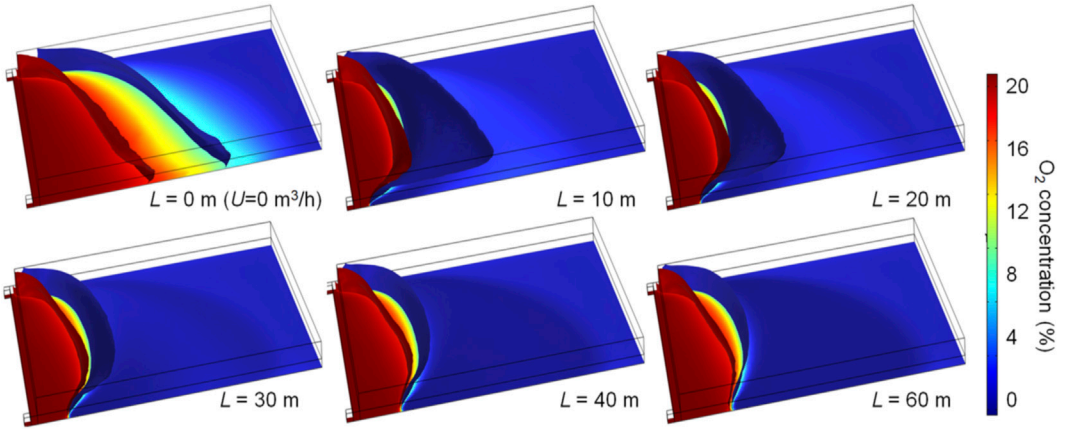

FIGURE 12
Simulated oxidation zone with different burial depths at U = 540 m^3 h^{-1}.

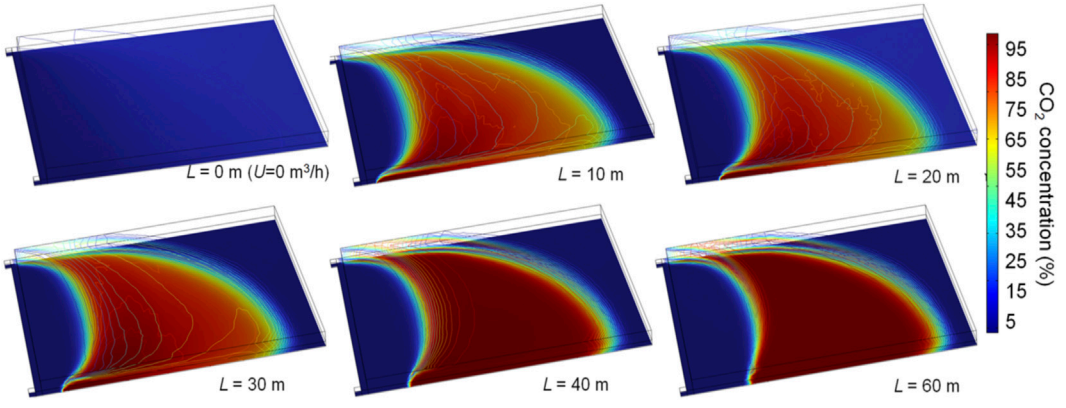

FIGURE 13
Simulated CO_2 distribution with different burial depths at U = 540 m^3 h^{-1}.

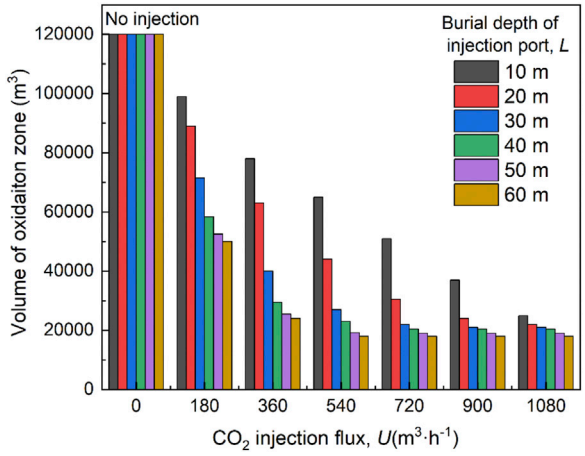

FIGURE 14
Predicted volume of the oxidation zone at different *L* and *U* values.

18,500 m^3 at Q=540 $m^3\ h^{-1}$, respectively. As L increases, the width of the oxidation zone in the upper area decreases rapidly. The volumes of the oxidation zone are almost identical at L = 50 and 60 m. In addition, the change in the burial depth of the injection port has little effect on the distribution of the oxidation zone on the return side.

5.5 Comprehensive analysis of coupling the CO_2 injection flux and location

Figure 14 shows the effects of coupling factors, that is, the CO_2 injection flux and location, on the predicted volume of the oxidation zone. A decrease in the CO_2 injection volume or burial depth of the port will reduce the volume of the oxidation zone. When U < 720 $m^3\ h^{-1}$, an increase in the burial depth significantly reduces the volume of the oxidation zone, especially at a lower injection flux. When U=1080 $m^3\ h^{-1}$, the change in the position of the injection port does not have a significant effect on the distribution of the oxidation zone. At L = 10 m, the volume of the oxidation zone decreases linearly with the injection flux. However, when L > 30 m, the volume dramatically reduces with increasing U from 0 to 540 $m^3\ h^{-1}$, but changes little as flux continues increasing. In practice, longer gas injection lines are avoided, which can make operations difficult. Smaller U values can save costs and reduce CO_2 concentrations in the upper corner and working face when achieving similar effects of suppressing coal spontaneous combustion for different U values. Therefore, based on the simulation results, the parameters of U = 540–720 $m^3\ h^{-1}$ and L = 30–40 m are recommended for the 5011 working face.

6 Conclusion

To accurately predict the effectiveness of CO_2 injection on spontaneous combustion in the coal mine gob. A mathematical simulation by COMSOL Multiphysics was applied in this study.

According to the conditions of the 5011 working face in the Tanyaoping coal mine, a 3-D mathematical model considering fluid-solid-thermal inter-relationship was established. The coal oxidation kinetic model was derived from the adiabatic oxidation test, where four stages were considered in the model. The apparent activation energies of the four stages are 143.25, 57.45, 32.89, and 19.48 kJ mol^{-1}, respectively. A good agreement between the field measurement and numerical simulation indicates the rationality of the mathematical model. CO_2 injection can dilute the O_2 concentration and prevent spontaneous combustion of coal. The coupling effects of injection flux, U, and the burial depth of the injection port, L, on the oxidation zone were investigated. The oxidation zone volume decreased with increasing U and L. When U or L is small, the upper width of the oxidation zone is wider, and as U or L increases, the upper width gradually decreases until it is no longer sensitive to parameter changes. An optimum injection plan is to keep the volume of the oxidation zone at a lower value in consideration of economic viability and operational parameters. The injection parameters of U = 540–720 $m^3\ h^{-1}$ and L = 30–40 m are recommended after considering the activity of the 5100 working face. The volume of the oxidation zone was estimated to be 18,500–23000 m^3.

Data availability statement

The original contributions presented in the study are included in the article/supplementary material, further inquiries can be directed to the corresponding author.

Author contributions

Investigation, methodology, writing—original draft, formal analysis, and final draft were completed by the author FJ.

Conflict of interest

The author declares that the research was conducted in the absence of any commercial or financial relationships that could be construed as a potential conflict of interest.

Publisher's note

References

Chu, T., Li, P., and Chen, Y. (2019). Risk assessment of gas control and spontaneous combustion of coal under gas drainage of an upper tunnel. *Int. J. Min. Sci. Technol.* 29 (3), 491–498. doi:10.1016/j.ijmst.2018.05.002

Deng, J., Lei, C., Xiao, Y., Cao, K., Ma, L., Wang, W., et al. (2018). Determination and prediction on "three zones" of coal spontaneous combustion in a gob of fully mechanized caving face. *Fuel* 211, 458–470. doi:10.1016/j.fuel.2017.09.027

Dou, G., Liu, J., Jiang, Z., Jian, H., and Zhong, X. (2022). Preparation and characterization of a lignin based hydrogel inhibitor on coal spontaneous combustion. *Fuel* 308, 122074. doi:10.1016/j.fuel.2021.122074

Guan, C., Liu, S., Li, C., Wang, Y., and Zhao, Y. (2018). The temperature effect on the methane and CO_2 adsorption capacities of Illinois coal. *Fuel* 211, 241–250. doi:10.1016/j.fuel.2017.09.046

Han, C., Nie, S., Liu, Z., Liu, S., Zhang, H., Li, J., et al. (2022). A novel biomass sodium alginate gel foam to inhibit the spontaneous combustion of coal. *Fuel* 314, 122779. doi:10.1016/j.fuel.2021.122779

Huang, Z., Quan, S., Hu, X., Zhang, Y., Gao, Y., Ji, Y., et al. (2022). Study on the preparation and inhibition mechanism of intumescent nanogel for preventing the spontaneous combustion of coal. *Fuel* 310, 122240. doi:10.1016/j.fuel.2021.122240

Li, J., Li, X., Liu, C., and Zhang, N. (2022). Study on the air leakage characteristics of a goaf in a shallow coal seam and spontaneous combustion prevention and control strategies for residual coal. *Plos one* 17 (6), e0269822. doi:10.1371/journal.pone.0269822

Liang, Y., Tian, F., Guo, B., and Liu, Z. (2021). Experimental investigation on microstructure evolution and spontaneous combustion properties of aerobic heated coal. *Fuel* 306, 121766. doi:10.1016/j.fuel.2021.121766

Lu, W., Cao, Y. J., and Tien, J. C. (2017). Method for prevention and control of spontaneous combustion of coal seam and its application in mining field. *Int. J. Min. Sci. Technol.* 27 (5), 839–846. doi:10.1016/j.ijmst.2017.07.018

Lu, W., Guo, B., Qi, G., Cheng, W., and Yang, W. (2020). Experimental study on the effect of preinhibition temperature on the spontaneous combustion of coal based on an $MgCl_2$ solution. *Fuel* 265, 117032. doi:10.1016/j.fuel.2020.117032

Lu, W., Zhang, X., Yuan, Y., Qi, G., Hu, X., Li, J., et al. (2021). Study on the characteristics and mechanism of a new type of antioxidant gel foam for coal spontaneous combustion prevention. *Colloids Surfaces A Physicochem. Eng. Aspects* 628, 127254. doi:10.1016/j.colsurfa.2021.127254

Lu, X., Zhu, H., Wang, D., Hu, C., Zhao, H., and Huo, Y. (2018). Flow characteristic investigation of inhibition foam used for fire extinguishment in the underground goaf. *Process Saf. Environ. Prot.* 116, 159–168. doi:10.1016/j.psep.2018.02.005

Ma, L., Guo, R., Wu, M., Wang, W., Ren, L., and Wei, G. (2020). Determination on the hazard zone of spontaneous coal combustion in the adjacent gob of different mining stages. *Process Saf. Environ. Prot.* 142, 370–379. doi:10.1016/j.psep.2020.06.035

Qi, Y., Wang, W., Qi, Q., Ning, Z., and Yao, Y. (2021). Distribution of spontaneous combustion three zones and optimization of nitrogen injection location in the goaf of a fully mechanized top coal caving face. *Plos one* 16 (9), e0256911. doi:10.1371/journal.pone.0256911

Qin, B., Li, L., Ma, D., Lu, Y., Zhong, X., and Jia, Y. (2016). Control technology for the avoidance of the simultaneous occurrence of a methane explosion and spontaneous coal combustion in a coal mine: A case study. *Process Saf. Environ. Prot.* 103, 203–211. doi:10.1016/j.psep.2016.07.005

Qu, L., Liu, L., Chen, J., and Wang, Z. (2023). Molecular model construction and optimization study of gas coal in the huainan mining area. *Processes* 11, 73. doi:10.3390/pr11010073

Si, J., Li, L., Cheng, G., Shao, H., Wang, Y., and Li, Z. (2021). Characteristics and Safety of CO_2 for the fire prevention technology with gob-Side entry retaining in goaf. *ACS Omega* 6 (28), 18518–18526. doi:10.1021/acsomega.1c02836

Sun, L., Zhan, M., Zhang, C., Shi, Q., Huang, Q., and Wang, W. (2022). Experimental study on prevention of spontaneous combustion of coal by ionic surfactant solution injection in coal seam. *Energy* 260, 125079. doi:10.1016/j.energy.2022.125079

Taraba, B., Michalec, Z., Michalcová, V., Blejchař, T., Bojko, M., and Kozubková, M. (2014). CFD simulations of the effect of wind on the spontaneous heating of coal stockpiles. *Fuel* 118, 107–112. doi:10.1016/j.fuel.2013.10.064

Wang, D., Zhong, X., Gu, J., and Qi, X. (2010). Changes in active functional groups during low-temperature oxidation of coal. *Min. Sci. Technol.* 20 (1), 35–40. doi:10.1016/s1674-5264(09)60157-5

Xia, T., Wang, X., Zhou, F., Kang, J., Liu, J., and Gao, F. (2015). Evolution of coal self-heating processes in longwall gob areas. *Int. J. Heat Mass Transf.* 86, 861–868. doi:10.1016/j.ijheatmasstransfer.2015.03.072

Xia, T., Zhou, F., Wang, X., Zhang, Y., Li, Y., Kang, J., et al. (2016). Controlling factors of symbiotic disaster between coal gas and spontaneous combustion in longwall mining gobs. *Fuel* 182, 886–896. doi:10.1016/j.fuel.2016.05.090

Xu, Y., Li, Z., Liu, H., Zhai, X., Li, R., Song, P., et al. (2020). A model for assessing the compound risk represented by spontaneous coal combustion and methane emission in a gob. *J. Clean. Prod.* 273, 122925. doi:10.1016/j.jclepro.2020.122925

Yoruk, B., and Arisoy, A. (2022). Development of a mathematical model for simulating the self-heating behavior of moist coal. *Combust. Sci. Technol.* 194 (13), 2674–2692. doi:10.1080/00102202.2021.1885388

Zhang, C., Wang, E., Xu, J., and Peng, S. (2021). A new method for coal and gas outburst prediction and prevention based on the fragmentation of ejected coal. *Fuel* 287, 119493. doi:10.1016/j.fuel.2020.119493

Zhang, H., Sasaki, K., Zhang, X., Sugai, Y., and Wang, Y. (2019). Numerical simulations on the self-heating behaviours of coal piles considering aging effect. *Combust. Theory Model.* 23 (6), 1169–1190. doi:10.1080/13647830.2019.1644378

Zhang, H., Wang, Y., Zhang, X., Sasaki, K., Sugai, Y., Han, F., et al. (2023). Experimental study of moisture effects on spontaneous combustion of Baiyinhua lignite from individual particles to stockpile. *Fuel* 334, 126774. doi:10.1016/j.fuel.2022.126774

Zhang, H., Zhang, X., Wang, Y., Dong, W., Fan, J., and Sasaki, K. (2022). Application of aging effect model in numerical simulation for predicting spontaneous combustion of coal stockpiles. *J. Therm. Analysis Calorim.* 147, 13847–13860. doi:10.1007/s10973-022-11708-7

Zhang, J., An, J., Wen, Z., Zhang, K., Pan, R., and Akter Al Mamun, N. (2020). Numerical investigation of coal self-heating in longwall goaf considering airflow leakage from mining induced crack. *Process Saf. Environ. Prot.* 134, 353–370. doi:10.1016/j.psep.2019.12.025

Zhang, Q., Hu, X. M., Wu, M. Y., Zhao, Y. Y., and Yu, C. (2018). Effects of different catalysts on the structure and properties of polyurethane/water glass grouting materials. *J. Appl. Polym. Sci.* 135 (27), 46460–46511. doi:10.1002/app.46460

Zhu, X., and Wen, H. (2023). Numerical simulation study on the influence of air leakage on oxygen concentration in goafs of fully mechanized caving mining with shallow buried and large mining height. *Front. Earth Sci.* 11, 281. doi:10.3389/feart.2023.1138925